ACS APPLIED NANO MATERIALS

www.acsanm.org Article

Doublet Nanoplate Structure of *Phoroncidia rubroargentea* Spider-Derived Guanine Crystals for Enhanced Broadband Reflectivity

Jinjin Zhong, Ling Li, Sarah Kariko, Long Zhang, Zhengyong Song, Xiang Li, Yuer Lu, Zhengdong Cheng,* and Jianwei Shuai*

Cite This: *ACS Appl. Nano Mater.* 2024, 7, 6487−6498 Read Online

ACCESS | Metrics & More | Article Recommendations | Supporting Information

ABSTRACT: Biogenic guanine nanocrystal-based multilayers offer intriguing biological structural models for designing dielectric optical systems with extraordinary optical effects, such as polarizing-insensitive broadband reflections and tunable and dynamic structural colors. Single crystals and crystals of nonmonocrystalline structures have been identified for biogenic guanine crystals. Although biogenic guanine crystals have been intensively investigated in relevant structure−function relationships, the role of various nonmonocrystalline structures of biogenic guanine crystals remains to be further explored. Here, we examine a doublet structure of the guanine crystal nanoplates responsible for the epidermal silvery coloration in a model spider, *Phoroncidia rubroargentea*, in both two and three dimensions. This doublet structure is composed of two tightly adhered crystallized layers. Half- and full-thickness defects are observed in these crystals. Combining structural characterizations and finite-difference time-domain (FDTD) optical modeling, here, we report a prospective role of this doublet structure. Simulation results indicate that defects in the doublet crystal nanoplates allow for enhancing light reflectance in the short-wavelength region while maintaining high reflectance at longer wavelengths for this natural optical system, as well as reducing the polarization degree of the reflected light in the visible range. Compared with previously reported undefined thickness variations of the nanocrystals for silvery coloration, this doublet structure provides an alternative strategy to optimize the broadband reflection in a more controllable way. This study also paves an avenue for structural optical design with guanine crystals at the individual crystal level.

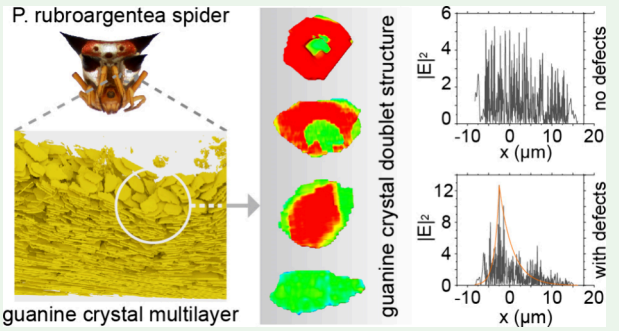

KEYWORDS: *guanine crystal doublets, half- and full-thickness defect, additional degrees of freedom, optical design, at the individual crystal level*

INTRODUCTION

By the advantage of high refractive index, biocompatibility and environmental compatibility, and magnetic stimuli-responsive property, biogenic guanine nanocrystals hold great potential in bioinspired optical design and fabrications.[1−11] Guanine, as a readily available nitrogenous metabolite in organisms, is used in many biofunctional assemblies of crystals.[12−17] Thin-plate guanine crystals of nanoscale thickness are responsible for a wide range of extraordinary optical phenomena, such as polarizing-insensitive broadband reflections[18,19] and tunable and dynamic structural colors.[20−23] Guanine crystals found in natural biological systems have all been determined to be anhydrous β polymorph (P1121/b, a = 3.59 Å, b = 9.72 Å, c = 18.34 Å, β = 119.5°),[24] and the biogenic guanine crystals of thin-plate morphologies have the (100) face as their largest surface resulting in a higher in-plane refractive index (n = 1.83) than in the normal direction (n = 1.46).[25] Besides the biological control over the crystallographic characteristics of the guanine crystals, various strategies have been evolved to develop different guanine crystal structures to facilitate related biofunctions in organisms. Understanding the structure−function relations is vital for relevant bioinspired assemblies for potential applications.

In the surface of many fish,[16,23,26−28] some spiders,[1,12,19,29] and copepods,[20,21,30] and the tapetum of fish,[31] scallops,[13,32,33] and spiders,[12,34−38] guanine crystal nanoplates have been found to form dielectric multilayers with intermediating cytoplasm between the crystals. These guanine nanocrystal-based multilayers often serve as various optical systems in relevant organisms, such as narrowband and broadband reflectors,[1,25] tunable photonic crystals,[5,22,23,28,39] and image-forming mirrors.[13] For these biogenic guanine crystal nanoplates, mono-, double-, and triple-layered structures have been

Received: January 12, 2024
Revised: February 26, 2024
Accepted: February 27, 2024
Published: March 7, 2024

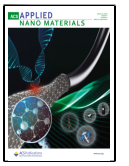

https://doi.org/10.1021/acsanm.4c00252
ACS Appl. Nano Mater. 2024, 7, 6487−6498

reported. In previous reports, the guanine crystal doublets refer to the crystals that contain two crystalline layers in a crystal. The previously reported doublet structures of guanine crystals encompass various configurations. These include the triple-layered structures observed in thin-plate crystals, with two crystalline layers and one intermediate layer consisting of amorphous components, which are responsible for the silvery structural coloration observed in certain spider species.[12] Additionally, the triple-layered structures found in prismatic crystals contributes to the white color exhibited by white widow spiders.[40] Moreover, the guanine crystals responsible for the sparkling color displayed by the Nudibranch *Flabellina iodinea* feature a double-layered structure of crystal nanoplates with two crystalline layers.[14] Aside from these guanine crystal doublets, biogenic guanine crystals with three crystalline layers have also been found to function as reflective components in some biological systems. These crystals exhibit well-defined platy morphologies with nanometer-scale thickness, including hexagon-shaped guanine crystals found in the surface of copepods[20,21] and square-shaped crystals in scallop eyes.[13,32] These regularly shaped crystals are also arranged in high order.[20,32] The regular hexagon or square shapes of these triple-layered guanine crystals could enable their tiling coverage to form a perfect narrowband reflector. The formation of such regular shapes has been suggested to derive from twinning or templating effects.[41−43] Relevant structure−function studies suggest that such regular and ordered assemblies have been biologically selected to facilitate communication among the same species, attraction of prey, intimidation of predators, or enhancement of vision in dark environment.[20,44,45]

Unlike the narrowband reflectors composed of guanine crystals with three crystalline layers, thin-plate guanine crystal doublets that have been found in nature all exhibit irregular shapes.[12,14,46,47] These guanine crystal doublets have been identified as high-refractive-index elements in broad-band reflective biological systems. Unlike narrowband reflectors, the morphologies and spatial arrangements of these guanine crystal doublets exhibit varying degrees of irregularity in broadband reflective biological systems. The natural broad-band silvery reflections observed on the surfaces of fish and spiders serve as important camouflage mechanisms against predators.[25,48,49] Previous studies reported that various strategies have been evolved across different species to reach similar reflective efficiencies for the broadband silvery reflections.[12] Among the guanine-based broadband reflectors, the structures of guanine crystals are mostly single crystals, which have been intensively studied in terms of both the formation mechanisms and the structure−function relationships. Little is known about the role of the doublet structure in biogenic guanine crystals. In the case of the spider species *Tetragnatha extensa*, the guanine crystal doublet was reported to exploit increased thickness to achieve similar reflective properties with fewer crystal layers, thus enhancing the reflective efficiency.[12] In this study, we present a potential role of the doublet structure of biogenic guanine crystals in the spider species *Phoroncidia rubroargentea*, which might be a previously undisclosed strategy for optimizing broadband reflectivity.

In this study, we investigated the doublet structure of guanine crystals in the epidermal silvery reflection system of the model spider *Phoroncidia rubroargentea*. First, we characterized this doublet structure in both two and three dimensions using transmission and scanning electron microscopy, along with automatic serial microtoming. We further conducted optical modeling with both ideally parallel crystal layer models and actual structural models based on the sampled complete multilayer from imaging. Our findings demonstrate that this doublet structure has the potential to offer additional degrees of freedom to enhance light reflectance in the short-wavelength region while maintaining high reflectance at longer wavelengths in the visible light range, thus optimizing broadband reflection for the model spider's epidermal reflection system. Additionally, the optical modeling also indicated that defects present in the crystal doublets significantly influence the polarization degree of the reflected light from guanine crystal-based multilayers. This study yields novel insights into the role of doublet structures in guanine crystals within biological systems and establishes a foundation for bioinspired ultrastructural optical design employing guanine crystals at the individual crystal level. Notably, owing to their biocompatibility and environmental compatibility, as wells as mechanical flexibility, guanine crystals hold great potential for advanced optical design and fabrication, including metasurfaces and metamaterials. The doublet structure, as compared to single crystals of guanine, enables optical design at the individual crystal level while enhancing flexibility in controlling the structure to explore more desirable optical properties.

EXPERIMENTAL DETAILS AND METHODS

Samples and Optical Imaging. We obtained specimens from collections of the Museum of Comparative Zoology (MCZ) and the California Academy of Sciences (CAS). The specimens used in this study were as follows: MCZ IZ 143122, 32022, 50966, 53933, 54189; CASENT 9057540, 9003201, 9057570, 9057533, 9057528, 9057542, 9057554, 9057519, 9057544, 9002297, 9002378, 9002420, 9003465. These specimens were stored in 70−80% ethanol prior to experiments. The remains of these specimens after the experiments were conducted are stored in their respective institutions. Images of MCZ specimens are credited to the Museum of Comparative Zoology at Harvard University.

The specimens were carefully cleaned by gently agitating them in vials of 70% ethanol and by removing debris with soft-tipped brushes. To prepare the spiders for optical imaging (MCZ IZ specimen 50966), they were positioned using featherweight forceps and watercolor paintbrushes and photographed using a Leica MZ 12 microscope with a Leica Plan Apo 1.6× objective lens connected by a Leica 0.63× mount connector. A JVC 3CCD digital camera was attached to the microscope to capture the images.

Electron Microscopy. MCZ IZ specimen 50966 was used for scanning electron microscopy (SEM) imaging using a Helios NanoLab 660 DualBeam electron microscope (FEI, OR) at an acceleration voltage of 5 kV and a working distance of approximately 4 mm. Prior to the SEM imaging, the spider sample was coated with Au or ultrathin carbon to reduce charging effects.

In order to prepare TEM and SEM samples with microtoming, spiders (CASENT 9057540) were embedded and prepared using a standard technique for microtoming. The rehydration process was done sequentially, starting from the original 70% ethanol to 50% ethanol for 30 min, to 30% ethanol for 40 min, and finally to water for 20 min. The specimen was then punctured between the two anterior spines and above the base of the pedicel before being fixed in a solution of 4% paraformaldehyde, 1% glutaraldehyde, and 0.1 M HEPES overnight. After fixation, the specimen was washed with 0.1 M HEPES three times and then four times with Milli-Q water on ice for 15 min each time. The process of dehydration was then done sequentially with increasing concentrations of ethanol at low temperatures, starting with 50% ethanol for 45 min, followed by 70% ethanol at −20 °C for 30 min and 95% ethanol at −20 °C for 30

https://doi.org/10.1021/acsanm.4c00252
ACS Appl. Nano Mater. 2024, 7, 6487−6498

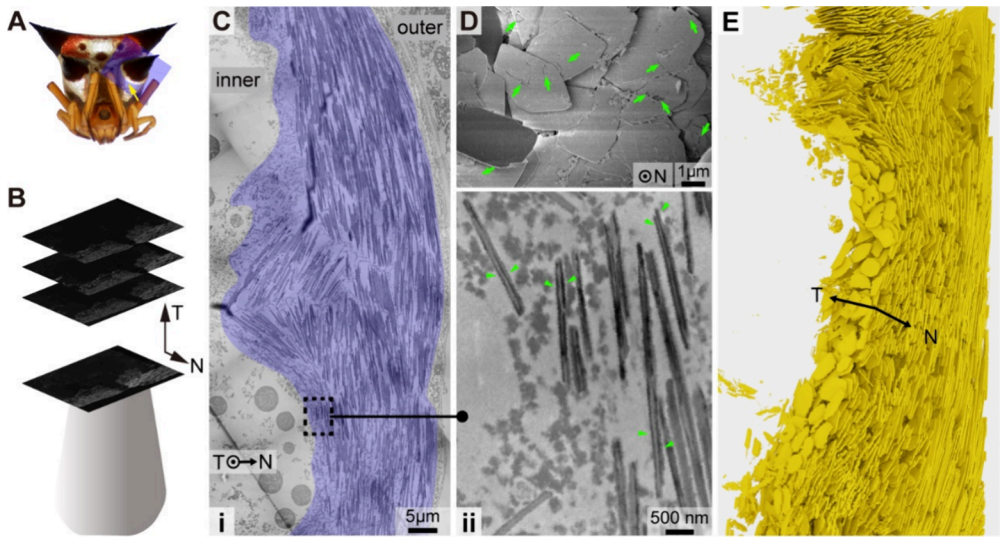

Figure 1. Guanine crystal doublets comprising multilayers responsible for the epidermal silvery coloration of the spider, *Phoroncidia rubroargentea*. (A) Front-view optical image of the spider specimen (MCZ IZ 50966). (B) Schematic diagram for the microtoming slicing along the cross section of the silvery part above the base of the spine, with N and T denoting the blade displacement direction in the slicing process and the normal of the cuticle surface, respectively. N and T were uniformly used in this study. (C) (i) TEM image of a cross section of a localized region with complete guanine crystal arrays from the interior to the edge side of the guanocytes (CASENT 9057540); (ii) an enlarged region within the black frame in (i). The green arrow heads point at the singlets composing four exemplified crystal individuals, which show distinct boundaries between the two singlets in a doublet structure. (D) Top-viewed SEM image of a localized region along the N direction of the multilayer, showing defects with different sizes, shapes, and locations in the crystals (MCZ IZ 50966). (E) Three-dimensional volume reconstruction of an exemplified guanine crystal multilayer structure.

min. The spider sample was infiltrated with an ethanol/London Resin (LR) white mixture with increasing resin concentrations, starting with 1:1 ethanol:LR white at −20 °C overnight, followed by 7:3 ethanol:LR white at −20 °C for 1 h and LR white at −20 °C for 1 h. For the final polymerization step, the spider specimen was placed in an oven-dried gel capsule with her spines pointing down at −50 °C overnight in an oven (Yamato DX300 Gravity convection). Once polymerized, the gel capsule was removed and the bottom of the resin block was trimmed with a razor blade before preparing slices using a Leica Ultratomicrotome UCT. The typical slice thickness was 50 to 80 nm for TEM imaging. The TEM imaging was carried out using a JEOL 2011 instrument operated at 120 kV with standard bright-field techniques. Using the technique of serial microtoming in combination with high-resolution serial-section electron microscopy (ssEM), we took serial images of the cross sections of the silvery reflection system. The subject silvery region was automatically sliced into thin sections at a step length of 65 nm by using the automated serial microtome technique. The images of as-obtained cross sections were taken by high-resolution scanning electron microscopy (SEM) imaging with a pixel size of 8 × 8 nm. To resolve the contradiction between high resolution and the coverage of several guanocytes, the images for different parts of one physical slice were taken, respectively.

Image Processing for Structural Characterization. For two- and three-dimensional structural characterizations, the obtained different section images for one physical slice were stitched together to get a complete image for the physical slice and then alignment was done on all the slice images to get the image series for the subject silvery region. The stitching and alignment were done in the TrakEM project in ImageJ. For the three-dimensional structural characterizations, the image segmentation was done in ImageJ and the volume reconstructions and the final rendering were realized in Avizo and Blender, respectively. The quantitative three-dimensional color mapping of the thickness of the guanine crystal plates was done using Avizo, based on image segmentation and identification of each individual guanine crystal as one entity for structural analysis. Measuring of the cytoplasm spacing in this study was performed using ImageJ.

Optical Modeling. The optical simulations in this study were conducted using the finite-difference time-domain (FDTD) method implemented with Lumerical FDTD Solutions software. According to a previous study,[29] the guanine crystal doublets from the epidermal silvery reflection system in the model spider have a roughly constant thickness, which is measured to be 110 nm ±22.8 nm (n = 134, where n is the total crystal number for the sampling statistic), and were determined to have a (100) face as the preferentially expressed surface by electron diffraction patterns, which is the same with other plate-like biogenic guanine crystals that have been found in nature. In all of the simulation models, the optical properties of the guanine crystal doublets were appropriately configured. In accordance with the crystallographic characteristic, the refractive index was set to be 1.46 along the normal direction of the crystal plates and 1.83 in the in-plane direction. The thickness of the guanine crystals with a complete doublet structure was set to be 110 nm. To perform optical modeling based on the actual structure of the guanine crystal multilayer sampled from the model spider's epidermal silvery reflection system, image segmentation of the guanine crystals within the sampled region was initially carried out using ImageJ. Subsequently, a surface mesh .stl file of the real multilayer structure was generated using Avizo. This .stl file was then imported into Lumerical FDTD Solutions software. Each guanine crystal within the imported multilayer structure was reconstructed as an independent structural element with its position, inclination angle, and shapes kept unchanged. Birefringence orientations were assigned to each individual guanine crystal based on their inclination angles and the refractive index characteristics of the guanine crystals, i.e., 1.46 along the normal direction and 1.83 in the in-plane direction. The in-plane optic axes were uniformly and randomly generated. The FDTD optical modeling employed plane waves of light with the BFAST mode and perfectly matched layer (PML) boundary conditions. Since the optical properties of the cytoplasm resemble that of water, the refractive index of the cytoplasmic spacing between the guanine crystal layers was set to be 1.33 in all of the optical simulations conducted in this study.

https://doi.org/10.1021/acsanm.4c00252
ACS Appl. Nano Mater. 2024, 7, 6487−6498

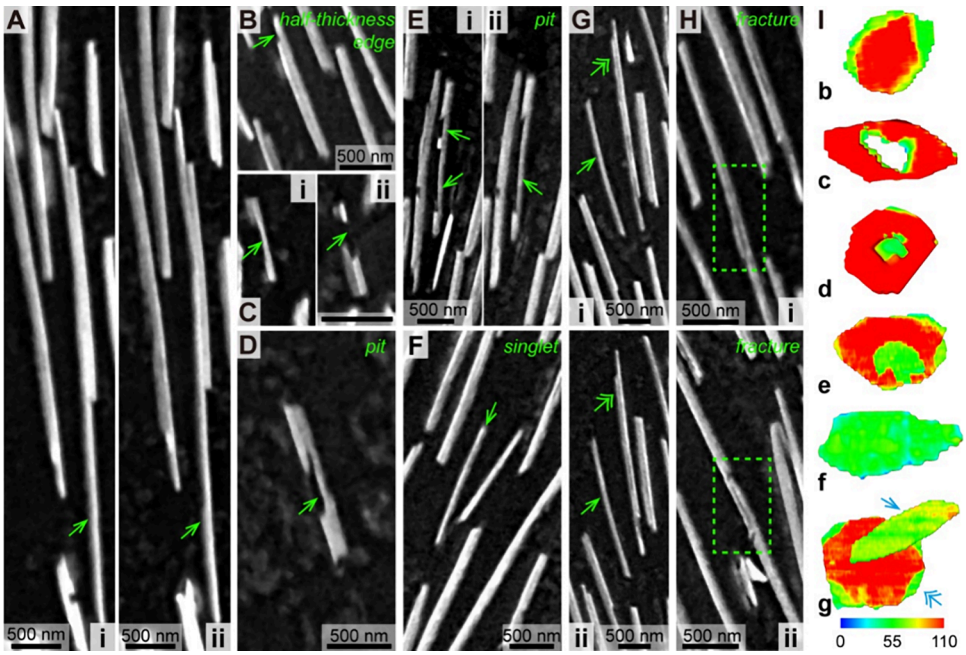

Figure 2. Half- and full-thickness defects in the guanine crystal doublets. (A, B) Two crystals with half-thickness edge: (A) (i, ii) two cross-sectional SEM images of one crystal indicated by the green arrow; (B) a cross-sectional SEM image of another crystal. (C) A crystal with a full-thickness hole in the crystal: (i, ii) two cross-sectional SEM images of the crystal; scale bar: 500 nm. (D) A cross-sectional SEM image of an individual guanine crystal with a half-thickness pit. (E) A guanine crystal with a more complex half-thickness defect pattern containing both pit and half-thickness edge: (i, ii) two cross-sectional SEM images of the crystal. (G) Two cross-sectional SEM images of a guanine crystal with half-thickness singlet and one crystal doublet with a half-thickness singlet structure, indicated by the green arrow and double arrows, respectively. (H) Two different crystals with physical fractures indicated by the green frames: (i, ii) a cross-sectional SEM image of the two crystals, respectively. (I) Color mapping of the thickness of the crystals in (b), (c), (d), (e), (f), and (g), corresponding to the crystals indicated by green arrows in (B), (C), (D), (E), (F), and (G), respectively.

RESULTS AND DISCUSSION

A Doublet Structure of the Biogenic Guanine Crystals in Spider, *Phoroncidia rubroargentea*. The guanine crystals investigated in this study are derived from the epidermal silvery reflection system located in the abdomen of the model spider *P. rubroargentea* (Figure 1A). This particular spider species has a habitat in the rainforest in Madagascar. Former research has already explored the underlying structural principles behind the coloration exhibited in the abdomen of the *Phoroncidia* spider.[29] The metallic silvery appearance observed in the spider's abdomen has been identified to result from guanine crystal-based multilayers. Thin slices of the silvery abdomen were obtained by using the microtoming technique, as depicted in Figure 1A,B. Figure 1C shows a representative region packed with guanine-crystal-based multilayers consisting of complete crystal layers extending from the interior to the edge of the guanocytes. Cross-sectional TEM images of the guanine crystals, primarily taken along the crystal plates' normal direction, reveal a distinct boundary between two closely adherent crystallized layers. Additionally, the SEM image depicted in Figure 1D, which offers a top-down view of the guanine crystals, demonstrates the frequent occurrence of defects in the crystal doublets. These guanine crystals form dielectric multilayer structures with an intermediating cytoplasm (Figure 1E), ultimately accounting for the epidermal silvery coloration of the model spider. Unlike standard photonic crystals, this natural dielectric multilayer reflector exhibits a lack of long-range order but possesses local orders.

From the cross-sectional SEM images of the guanine crystals (Figures 1C and 2A,B), offsets between the boundaries of the two crystalline layers within a crystal were frequently observed, which results in half-thickness edges and shows asymmetry between the two crystalline layers in terms of morphology. Notably, the guanine crystals also exhibit the presence of holes (Figure 2C) and pits (Figure 2D,E). The pits observed in the crystal doublets possess a thickness equivalent to that of a single crystalline layer. Singlets, which represent individual layers without their corresponding counterparts for a complete doublet structure, are also frequently observed within the multilayer structure (Figure 2F,G). In this study, we classify the missing components of holes as full-thickness defects, pits as pits, and incomplete edges within an otherwise complete crystal doublet as half-thickness defects. The strong bonding or high degree of crystallographic coordination between the two singlets in a crystal doublet may hinder the clear visibility of the doublet structure in some cross-sectional SEM images of the guanine crystals. Nonetheless, the occurrence of physical fracture patterns in such crystals still suggests the presence of an inherent doublet structure, as demonstrated in Figure 2H. Three-dimensional structural analyses and color mapping of crystal plate thickness further reveal that half-thickness edges and pits can assume diverse shapes and exhibit various area ratios within individual crystals (Figure 2I and Figures S1 and S2). Moreover, these half-thickness defects can occur at arbitrary positions within the crystals. Half-thickness defects are frequently observed in the crystal doublets (Figure S3) while full-thickness holes occur only sporadically in these crystals.

https://doi.org/10.1021/acsanm.4c00252
ACS Appl. Nano Mater. 2024, 7, 6487−6498

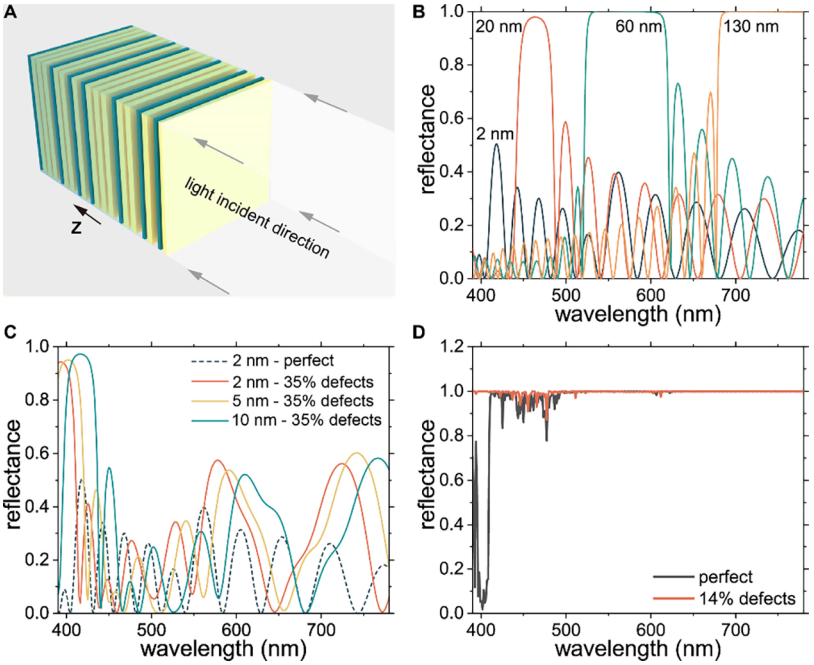

Figure 3. Visible-light reflectance from guanine crystal multilayers comprising either all pristine crystal layers or partial layers with crystals exhibiting half-thickness defects. (A) Schematic representation of guanine crystal multilayer reflectors with visible-light incident perpendicular to the crystal plates. Yellow and blue indicate guanine crystals without defects and with half-thickness defects, respectively, separated by cytoplasmic layers. The *Z* direction indicates the normal direction of ideally parallel multilayers, which is consistent throughout the manuscript. (B) Reflectance spectra for perfect guanine crystal multilayers (20 layers in total) with different cytoplasm spacings of 2, 20, 60, and 130 nm. (C) Reflectance spectra for multilayers (20 layers in total) composed of guanine crystals with different states. (D) Reflectance spectra comparison for an ideal multilayer model (120 layers in total) of perfect guanine crystals (black line) against a model with 14% of the layers having half-thickness defects (orange line). The number of guanine crystal layers is 20 for cytoplasm spacings of 2, 5, and 10 nm, respectively, and 10 for spacings of 20, 30, 40, 60, 100, and 140 nm, respectively.

We summarized the characteristics of the two-dimensional cross-sectional images and three-dimensional structural reconstructions of the guanine crystals in this model natural optical system, which reveal an intrinsic doublet structure of the biogenic guanine crystals. This doublet structure is indicated by (i) the presence of half-thickness edges in a crystal with the two crystalline layers spanning different sizes; (ii) physical fracture patterns in the center of the crystals; (iii) the occurrence of half-thickness pits and full-thickness holes within a crystal; and (iv) the presence of half-thickness singlets. Notably, the doublet structure observed in the guanine crystals within the silvery reflection system of the model spider abdomen differs significantly from previously reported doublet structures, which typically feature a sandwiched amorphous layer between two crystalline layers in some spider reflection systems.

Role of the Doublet Structure of Guanine Crystals in the Optical Performance. Natural guanine crystal nanoplate-based multilayer reflectors are specific variants of standard thin-film Bragg reflectors. Ideally parallel multilayers usually serve as basic models or building blocks extracted for studying relevant structure−function relationships in the sense of theoretical, methodological, and practical application implications. Based on ideally parallel models, thickness variation of either or both the crystal and cytoplasm spacing,[1,50,51] crystallographic structures of guanine crystals,[18,19] and inclination angles between different multilayer stacks[52] have all been studied as independent structural factors in the optical performance-derived structure−function relationship studies. Here, for the doublet structure of guanine crystals composing the epidermal silvery reflection system in the model spider, novel structural elements enabled by such a doublet structure, i.e., half- and full-thickness defects, are first observed. We first explored the optical performance of the guanine crystals in ideally parallel multilayer models considering half- and full-thickness defects as structural elements. Subsequently, we study an ideally parallel model to more closely simulate the natural configuration in the spider, including the layering number and cytoplasmic spacings based on the empirical measurements on a real structure sampled from the model spider. This model allows us to bridge the gap between idealized models and biological reality and provides a bioinspired configuration pattern. Finally, taking into consideration the integrated influence with other structural factors, such as the inclination angles, we take a step further to consider an authentic guanine crystal multilayer structure and evaluate the optical consequences of the presence or absence of crystal defects.

In the ideally parallel models, as depicted in the schematic (Figure 3A), the optical performance of the guanine crystal doublet-based multilayer reflectors exhibits significant variation, depending upon the state of the crystals, specifically with regard to the presence or absence of defect-related structural elements. With an intact guanine crystal doublet configuration and constant cytoplasmic interlayer spacing, the primary reflective band, or photonic band gap, exhibits a marked stability. However, the reflectance peak intensity increases concomitantly with the crystal layers, reaching a saturation point (Figure S4), just as previous studies have shown.[46] When the cytoplasmic spacing is altered from 2 to 140 nm, a redshift

https://doi.org/10.1021/acsanm.4c00252
ACS Appl. Nano Mater. 2024, 7, 6487−6498

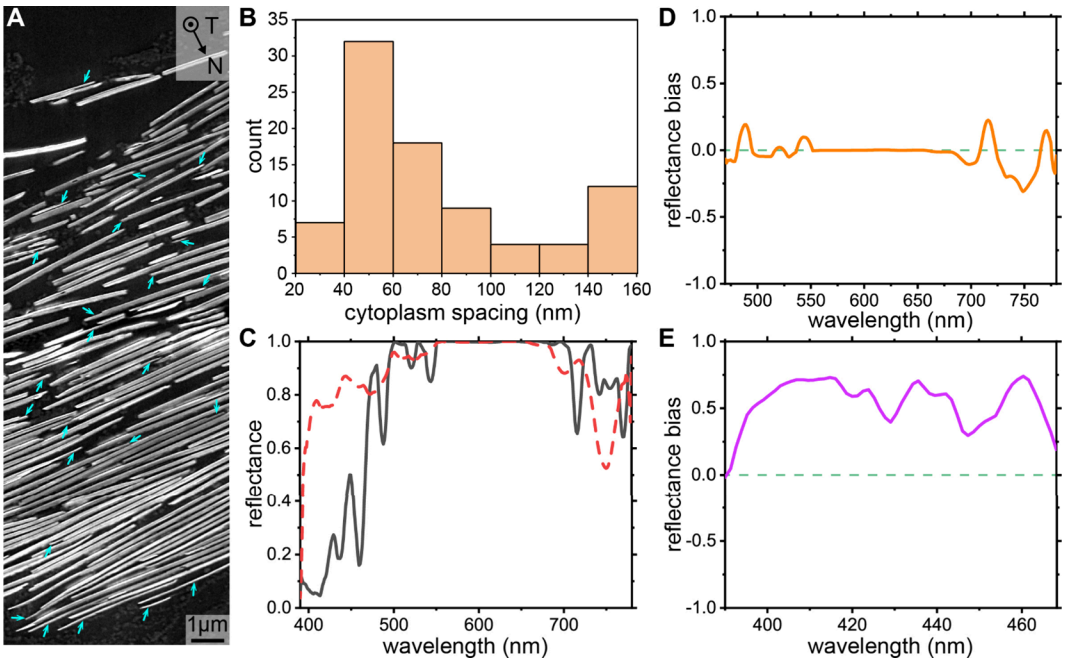

Figure 4. Optical modeling of an ideally parallel multilayer constructed based on statistical analysis of cytoplasm spacing in a sampled region of the silvery epidermal reflection system in the model spider. (A) Sampled guanine crystal-cytoplasm multilayer structure used for constructing the idealized model, with half-thickness defects indicated by cyan arrows. (B) Statistical distribution of cytoplasm spacing in the multilayer reflector shown in (A). (C) Reflectance spectrum of visible light (incidence angle ~0°) from the idealized model with perfect guanine crystals, considering 18% half-thickness defects. (D) Deviation of reflectance under the condition of 18% crystal defects compared to the perfect crystal state in the longer wavelength region (480 to 780 nm). (E) Deviation of reflectance under the condition of 18% crystal defects compared to the perfect crystal state in the shorter-wavelength region (390 to 480 nm).

in the main reflective band is noted, as evidenced in Figure 3B and Figure S5. Upon extending the cytoplasmic spacing further to 180 nm, the main reflective band abruptly transitions to a narrow band at shorter wavelengths. For spacings exceeding 180 nm, the main reflective band demonstrates a recurring shift toward longer wavelengths as the spacing is increased. Notably, while the main reflective band at a spacing of 170 nm persists at the longest wavelength observed, the secondary reflective peak manifests as a pronounced elevation within a confined spectral region at shorter wavelengths. To elucidate the nuanced spectral variations occurring between 130 and 160 nm, we adopted a reduced interval of 5 nm for computational analysis of the optical performance, as detailed in Figure S5. This approach was instrumental in determining whether the band of high reflectance could entirely span the range of shorter wavelengths.

The simulation results elucidate that the ideally parallel multilayers, comprising perfect guanine crystals, have the inherent ability to reflect the vast majority of the visible-light spectrum through the variation of cytoplasm spacing. The reflectance, however, is notably diminished within the short-wavelength region, as is clearly delineated in Figure 3B and Figure S5. Subsequent comparative simulations were conducted with the introduction of half-thickness defects in the crystals. As shown in Figure 3C, the inclusion of defects within the guanine crystals broadens the high-reflectance band achievable by the multilayer structure, encompassing even the shortest-wavelength region, a spectral domain unachievable in defect-free crystal configurations.

A multilayer model with ideally parallel crystal layers was further constructed to cover presumably the widest high-reflection spectrum for the visible-light range based on the simulation results from Figure 3B and Figure S5. This modeling further substantiates, as demonstrated in Figure 3D, that the integration of half-thickness defects substantially enhances the otherwise diminished reflectance at shorter wavelengths observed in the perfect guanine crystal counterparts. Concurrently, it preserves the high reflectance at longer wavelengths. Such findings may unveil a hitherto unrecognized mechanism by which biological reflective systems achieve broadband reflectance across the visible spectrum. Specifically, biogenic guanine crystal doublets with defined thickness demonstrate a capacity for reflecting a substantial portion of the visible-light spectrum, albeit with reduced reflectance at the extreme short-wavelength end. Notably, this spectral gap in high reflectance at shorter wavelengths could be compensated by the presence of half-thickness defects within the crystal doublets. Such novel structural elements are hypothesized to facilitate a broadband silvery reflection, thus enhancing the overall reflective efficiency across the entire visible range.

While full-thickness holes are rarely observed in the biogenic guanine crystal doublets that constitute the model biological reflectors, these defects are important featured structural elements that emerge from this particular doublet conformation. A statistical analysis of the crystal size was conducted on 250 guanine crystal plates sampled from the epidermal guanine-based multilayer reflector in the model spider, with the Feret width employed as a representative measure (Figure S6). The average Feret width of the guanine crystal plates was determined to be approximately 2400 nm. Based on this knowledge, ideally parallel guanine crystal multilayer models were constructed to preliminarily explore the optical effects of holes of different dimensions within square plates with a side length of 2400 nm in comparison to the model with all-perfect

https://doi.org/10.1021/acsanm.4c00252
ACS Appl. Nano Mater. 2024, 7, 6487−6498

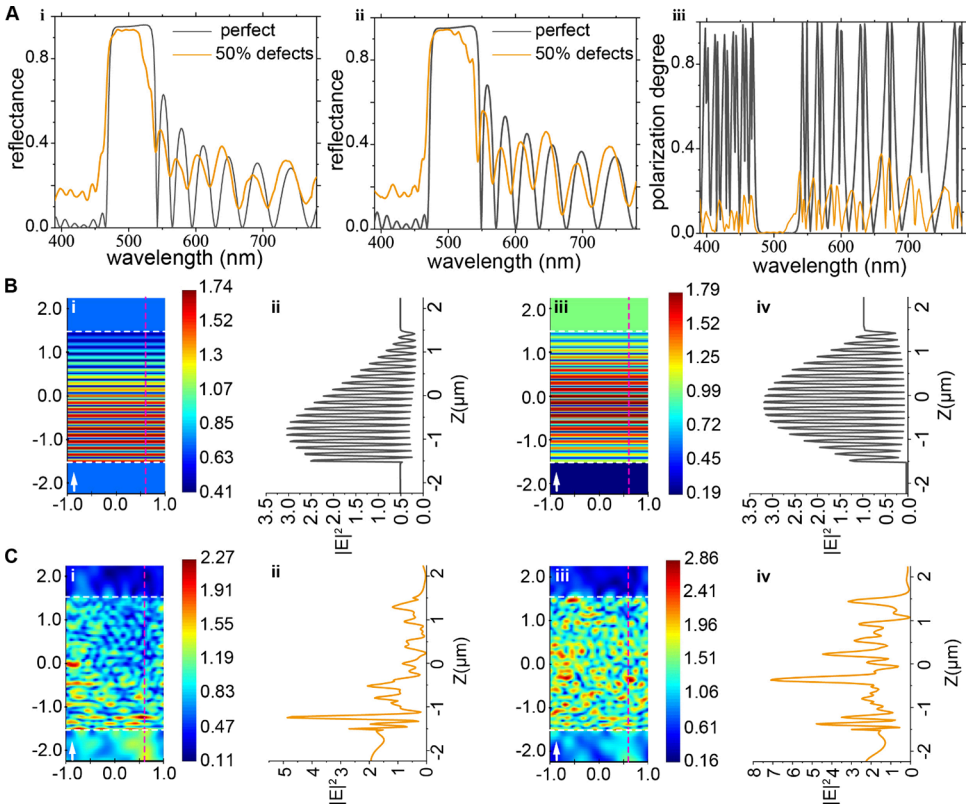

Figure 5. Reflection of light from the guanine crystal-based multilayer with the intermediating cytoplasm layers of 40 nm thickness under different states of the guanine crystals, for an incident angle of 20°. (A) Reflectance spectrum of the multilayer without crystal defects (indicated by the black line) and with a crystal defect ratio of 50% (indicated by the orange line), for *p*-polarized (i) and *s*-polarized (ii) light sources; (iii) spectrum of the polarization degree of the reflected light for the nonpolarized source from the multilayer without defects (black line) and with a crystal defect ratio of 50% (orange line). (B, C) Propagation of light with wavelength of 470 nm propagating in the multilayer without defects (B) and with 50% crystal defects (C); for *p*-polarized light: (i) electric field strength distribution and (ii) intensity profile taken along the *Z* direction following the wine dashed line in (i); for *s*-polarized light: (iii) electric field strength distribution and (iv) intensity profile taken along the *Z* direction following the wine dashed line in (iii). The arrow indicates the incident direction of light, and the white dashed lines represent the boundaries of the multilayer structure.

crystals. The FDTD optical modeling results show that the introduction of these full-thickness defects enables light reflection within the forbidden spectral regions under an all-perfect crystal state (Figure S7). Notably, it was observed that increasing the size of holes further enhances the reflectivity of some of the newly accessible bands, albeit at the expense of further lowering reflectance within the primary reflection band in the case of all-perfect crystals. The hole defects play a role in broadening the reflectivity of the narrowband reflective multilayer structure through enhancing the reflectivity in the otherwise forbidden spectral regions sitting at the two sides of the main reflection band.

In the actual structures of the model biological optical system, a complete multilayer structure responsible for the silvery reflection typically consists of fewer than 100 layers. We further constructed an ideally parallel model based on a statistical analysis of cytoplasm spacing in the crystal stacks from a specific sample region of the actual biological multilayer structure, as shown in Figure 4A. This statistic was made by measuring the spacing between the most adjacent crystals in different layers along the N direction. In inclined cases, the spacing was approximated as the distance between the center of the overlapping part of the two adjacent crystals. The ideally parallel multilayer model was constructed with the cytoplasm spacing according to the empirical measurements (Figure 4B). The perfect guanine crystal doublets roughly account for a large proportion of 82%. The modeling results demonstrate that the perfect crystal multilayer exhibits an even poorer performance in the short-wavelength region compared to the ideally parallel model described above (Figure 3D). However, the inclusion of a small fraction of 18% crystal defects significantly enhances the low reflectance in the short-wavelength region while maintaining relatively consistent reflectance levels at longer wavelengths (Figure 4C–E). The optical modeling based on the biomimetic configuration of the multilayer structure, which incorporates cytoplasmic interlayers and a quantity of crystal layers consistent with empirical observations, underscores the pivotal role of crystal defects in achieving broadband silvery reflectance.

In the realm of dielectric multilayer reflectors, the polarization characteristics of reflected light are critical for a range of practical applications[53,54] and biological functions.[34,55] The degree of polarization for reflected light is quantitatively defined as |Rp − Rs|/(Rp + Rs), where Rp and Rs represent the reflectance of *p*- and *s*-polarized light, respectively. At oblique incidence, the polarization effect can diminish the overall reflectance for an unpolarized light source. Certain species utilize polarized light reflections for critical biological processes such as interspecies communication, whereas organisms relying on broadband silvery coloration for camouflage necessitate polarization-insensitive reflections,

https://doi.org/10.1021/acsanm.4c00252
ACS Appl. Nano Mater. 2024, 7, 6487−6498

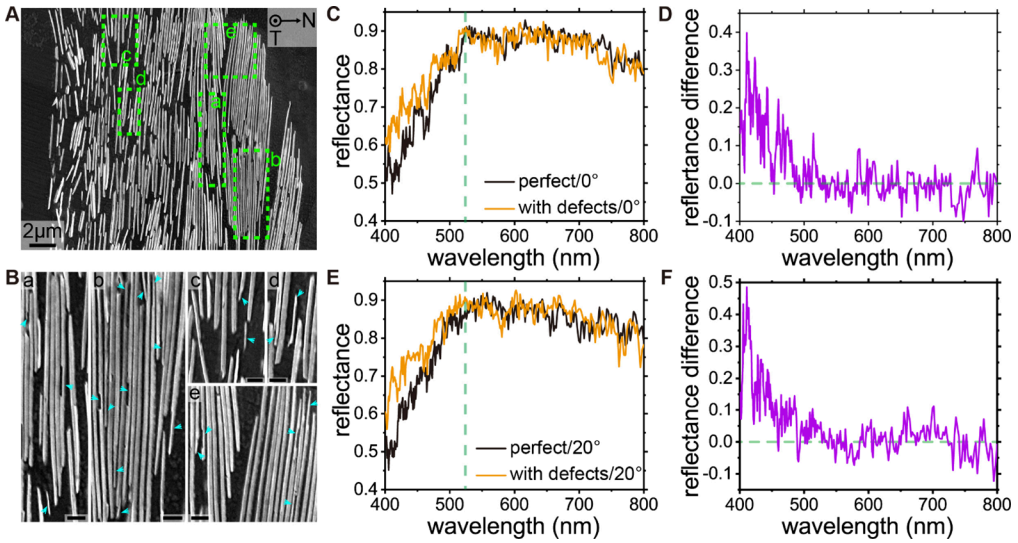

Figure 6. FDTD optical modeling of the visible-light reflections from a real guanine crystal-cytoplasm multilayer structure of a sampled guanine crystal-cytoplasm multilayer region in the silvery abdomen of the model spider with and without defects in the doublet structure of guanine crystals. (A) The sampled region of the original multilayer structure from the spider silvery reflection system in the abdomen for the geometry setup in the optical modeling. (B) Enlarged images for the local regions in (A) outlined by the green dashed lines: (a−e) corresponds to the local region (a−e) in (A). Cyan arrows indicate the frequently occurring half-thickness defects in the guanine crystals. Scale bar: 500 nm. (C−F) Visible-light reflectance spectrum from the multilayer model with perfect crystal structure (black line) and with defects considered (orange line): (C) incidence angle ∼0°. (D) The relative difference of reflectance for 0° incidence angle. (E) Incidence angle ∼20°. (F) The relative difference of reflectance for 20° incidence angle.

particularly at non-normal incidence angles, where a reduced polarization effect is beneficial.

We employed an ideally parallel multilayer model to investigate the impact of the crystal defects on the polarization property of guanine crystal-based multilayer reflectors. Simulations were performed to compare the visible-light reflections from the multilayer of entirely perfect crystals against those with 50% of crystals exhibiting defects (as depicted in Figure 5). The simulations demonstrated that the presence of crystal defects could enhance the reflectance of the original forbidden spectral bands observed in the structure of entirely perfect crystals in the multilayer. The incorporation of crystal defects tended to broaden the spectral region of reflection while significantly diminishing the polarization degree of reflected light for an unpolarized source on the whole, as compared to the scenario with all-perfect crystals (Figure 5A). Further investigations were aimed at understanding the underlying mechanism of the pronounced decrease in polarization degree observed upon the introduction of crystal defects. This was carried out by examining the light propagation within the multilayer structures by using a representative wavelength of 470 nm for both perfect and 50% defective multilayer configurations (Figure 5B,C). For the defect-free multilayer, the reflectance was calculated to be 50.57% for *p*-polarized light and only 3.55% for *s*-polarized light. For the multilayer with 50% defective crystals, the reflectance increased to 82.47% for *p*-polarized light and 69.06% for *s*-polarized light. Correspondingly, the degree of polarization was calculated to be 86.90% for the multilayer comprising solely perfect guanine crystals, compared to 8.84% for the assembly with 50% defective crystals. The highly polarized nature of the reflected light from the all-perfect guanine crystal multilayer was largely attributed to the diminished reflection of the *s*-polarized light.

The light propagation behavior characterized by the electric field intensity distribution in the multilayer structure reveals that the defect-free structure shows discrete and uniformly distributed electric field maxima across the layers, which are characteristic of the Bragg reflection condition and typical of high-quality dielectric mirrors designed for narrowband high reflectance at the specified wavelength. In contrast, the defective structure exhibits a complex field distribution with less pronounced peak uniformity along with regions of concentrated electric field strengths not aligned with the interfacial periodicity. In sum, the heightened reflectance associated with the defective structure could be rationalized by several nonexclusive mechanisms: (1) Defect-induced scattering may increase the path length of photons within the reflector, sustaining multiple internal reflections and enhancing the probability of reflection. (2) Localized defect modes within the multilayer structure might act as resonant cavities, trapping light and contributing to increased reflectance. (3) Defects could also disrupt destructive interference pathways, effectively reducing transmission losses and increasing overall reflectance.

The ideally parallel models demonstrate the ability of the doublet structure with defined thickness to realize broad-band silvery reflection through introduction of defects intrinsic to the crystal doublets. For the natural biological reflection systems, in view of the influence of the spatial arrangement of the guanine crystals on the optical performance in actual structures, we further conducted optical modeling based on the geometry of an actual complete multilayer structure obtained from imaging, as shown in Figure 6A. Figure 6B demonstrates the frequently occurring half-thickness defects observed in the guanine crystals comprising the actual multilayer structure. With the same spatial arrangement of the guanine crystals as observed in Figure 6A, the reflection system under the hypothetical perfect crystal state still shows a relatively low reflectance in the short-wavelength region. This can be

https://doi.org/10.1021/acsanm.4c00252
ACS Appl. Nano Mater. 2024, 7, 6487−6498

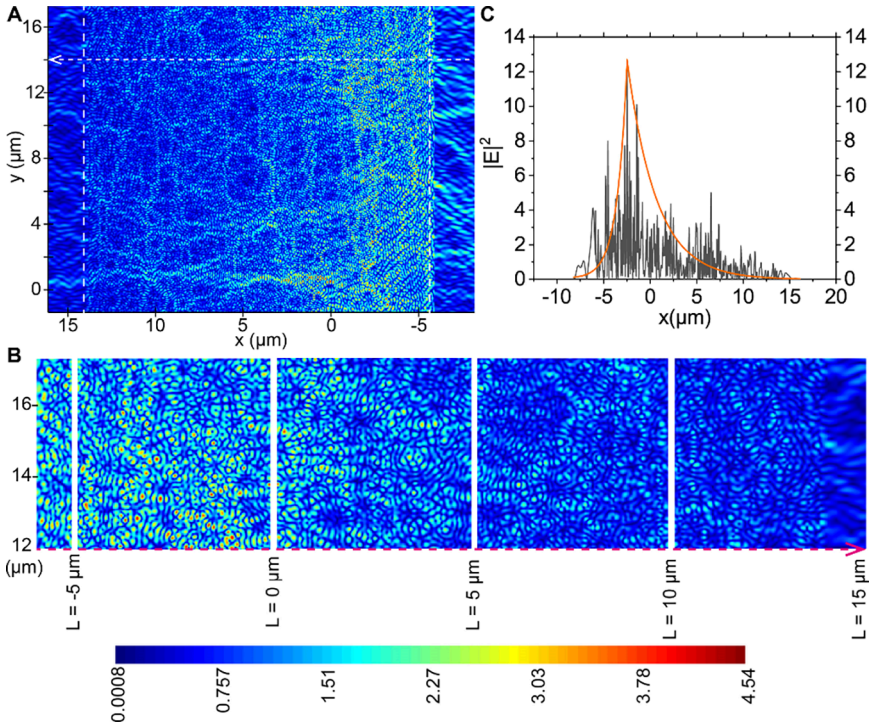

Figure 7. Transition to the localization of light with the incorporation of defects in the sampled multilayer region from the epidermal silvery reflection system of the model spider. (A) Electric field strength ($|E|$) distribution in the sampled multilayer region in Figure 4A for wavelength ~411 nm at incidence angle ~20°. The white dashed lines indicate the boundaries of the multilayer structure. (B) Enlarged images along the white arrow at every 5 μm. (C) The electric field intensity profile ($|E|^2$, black line) along the white arrow in (A), showing exponentially decaying on the whole by the orange line. The color bar indicates the electric field strength.

attributed mainly to the thickness of the guanine crystals, as inferred from the above idealized modeling results in Figure 3. However, when taking into consideration the defects identified in partial crystals, the light reflectance in the short-wavelength region, specifically on the left side of the green dashed line (Figure 6C,E) at a wavelength of 525 nm showed a significant enhancement while the high reflectance at longer wavelengths is maintained. The integration of the light reflectance in the short-wavelength region of the visible light below 525 nm was raised by magnitudes of 8.85 and 10.44% for the incidence angles of 0 and 20°, respectively. In contrast, the reflectance remained roughly at the same level and fluctuated by very small magnitudes in the longer-wavelength region. This observation suggests that the doublet structure may be one of the strategies utilized to optimize the efficiency of silvery reflections in nature. For reference, the standard silvery reflection spectrum is presented in Figure S8.

To investigate the enhancement of reflectance in the short-wavelength region caused by half-thickness defects, we selected a light wavelength of 411 nm and examined light propagation behavior under the two different conditions with and without defects in guanine crystal doublets. The presence of defects leads to a 48.5% increase in reflectance at this wavelength incident at 20° in the actual model (Figure 6F). The electric field intensity was calculated for light with the wavelength of 411 nm incident at 20° in the actual model, as illustrated in Figure 7 and Figure S9. In the case of perfect crystals, there were no significant changes in the electric field intensity within the range of 0 to 13 μm (Figure S9A,B). However, upon incorporating half-thickness defects into the crystals, the electric field was intensely distributed in the region from −5 to 0 μm, followed by a rapid decay in the direction of light propagation (Figure 7A,B). We examined the intensity profile ($(|E|^2)$) along the white arrow and observed that, in the perfect crystal state, the profile exhibited a Gaussian shape, indicating a diffusive propagation pattern predominance. Conversely, the exponential decaying intensity in Figure 7C suggests that the inclusion of half-thickness defects could lead to the localization of light, resulting in suppressed light transmission and enhanced reflectivity in the short-wavelength region of visible light.

Natural dielectric optical systems provide intriguing biological structural models for designing different bioinspired optical systems with extraordinary optical effects. Biogenic guanine crystals are one of the highest-refractive-index biological materials and are extensively used as an optical material in animals. By using the combination of microtoming and high-resolution serial-section electron microscopy (ssEM), we first revealed the assembly details of a doublet structure of biogenic guanine crystals in nanometers (Figures 1 and 2). This technique allows for three-dimensional structural reconstructions of individual guanine crystals and their spatial arrangement over a large region of several guanocytes in the model spider as well (Figure 1C,E). The structural details in nanometers clearly show that the guanine crystal is composed of two tightly adherent crystalline layers that form a doublet structure. The structural connection pattern between two crystalline layers is similar to that in the guanine crystal doublets in the Nudibranch *Flabellina iodinea*, but different from those in the crystal doublets in other previously identified spider species.

The systematic optical modeling shows that for the guanine crystal doublets identified in the *Phoroncidia rubroargentea* spider, light reflections exhibit low reflectance at short

https://doi.org/10.1021/acsanm.4c00252
ACS Appl. Nano Mater. 2024, 7, 6487−6498

wavelengths from the multilayer reflectors comprising of the guanine crystal doublets with the full thickness of the doublets (Figures 3 and 4), which would influence the actual optical performance requiring silvery reflections. The presence of half-thickness defects in the doublet structure could broaden the high-reflectance band to encompass the short wavelengths that would otherwise lie beyond the coverage range of multilayers composed of this guanine crystal (Figures 3C,D, and 4). Broadband high reflectance across the visible light range is desirable for the model spider's camouflage as dew drops. Through a combination of structural characterizations and systematic finite-difference time-domain (FDTD) optical modeling, we demonstrate that the defects observed in the crystal doublets may have been utilized by the model spider to optimize broadband high reflectance in the visible-light range. Specifically, the defects enhance reflectance in the short wavelength range while maintaining a high reflectance at longer wavelengths (Figure 6). In comparison to strategies employing guanine crystals with largely undefined thickness variations to achieve similar broadband silvery reflective properties in certain species,[47,48] the consistent thickness of guanine crystals offers an advantage in bioinspired fabrication and design due to its better controllability.

The half- and full-thickness defects are observed in the biogenic guanine crystal doublets in the epidermal silvery reflection system of the *Phoroncidia rubroargentea* spider. Since the experimental spider samples have been stored in fixative for several months, it is challenging to ascertain whether the half- and full-thickness defects in the guanine crystals are artifacts or occur naturally during the crystal growth process. As novel structural elements observed in biogenic guanine crystals, we first explored the effect of these defects in the crystal doublets on the optical performance of guanine crystal-based multilayer reflectors. The half- and full-thickness defects enabled by such a doublet structure not only show their crucial role in achieving the broadband reflection for the multilayer structure but also demonstrate that the dual layers of a crystal doublet can be manipulated to fine-tune the optical properties of bioinspired structures, opening new avenues for individual crystal-level structural customization. If these defects are indeed inherent to the growth process, then the presence of various defects in the guanine crystals indicates a significant degree of independence between the development of the two closely adherent crystalline layers in the doublet structure. The formation mechanism of such a doublet structure remains to be explored. Notably, guanine crystal, known for its environmental and biocompatibility as well as its responsiveness to magnetic stimuli, stands out as a promising optical material for practical applications. Drawing inspiration from the natural development of the guanine crystal doublet structure can greatly facilitate the bioinspired fabrication of guanine crystals. Moreover, with advancements in techniques for controlling the size, shape, and distribution of half-thickness defects, guanine crystals hold great potential for applications in advanced optical devices including 2D metasurfaces and 3D metamaterials.

CONCLUSIONS

Guanine nanocrystals, known for their high refractive index among biological materials, are widely employed in animals as scatterers, reflectors, and photonic crystals, contributing to a wide array of extraordinary natural optical phenomena. Understanding the assembly function relationships is of paramount importance for bioinspired designs and fabrications. Although doublet structures of guanine crystals have been identified in various species, their roles remain largely unexplored, despite extensive investigations on the structure–function relationships of biogenic guanine crystals. Here, we first revealed the structural details of a doublet structure of biogenic guanine crystal nanoplates in both two and three dimensions. These guanine crystals consist of two tightly adherent crystalline layers, responsible for the spider species *P. rubroargentea*'s silvery epidermal coloration. Compared to single-crystal structures, such a doublet structure allows for defects such as half-thick edges, pits, singlet plates, and full-thickness holes, which have been observed in the guanine crystals sampled from the model spiders. These defects create ample opportunities for bioinspired optical design utilizing guanine nanocrystals at the individual crystal level, which has also been preliminarily demonstrated by the optical modeling based on ideally parallel multilayer models in this study.

Through a combination of structural characterizations and finite-difference time-domain (FDTD) optical modeling, we demonstrate that the introduction of defects in the doublet structure can expand the high-reflection band of ideally parallel multilayers of these guanine crystals toward shorter wavelengths that would otherwise fall beyond the coverage of the high-reflection band. Moreover, for the authentic guanine-based multilayer reflectors in the model spider, the presence of defects in these guanine crystal nanoplates significantly alters the propagation behavior of light in the multilayer structures, leading to a localization mode that enhances reflectivity in the short-wavelength region of visible light while maintaining high reflectivity at longer wavelengths. This doublet structure may have been employed by the model spider to optimize silvery reflections for camouflage purposes.

ASSOCIATED CONTENT

Supporting Information

The Supporting Information is available free of charge at https://pubs.acs.org/doi/10.1021/acsanm.4c00252.

The SEM image sequences and volume rendering for several individual guanine crystals; two exemplifying regions showing guanine crystal multilayers with defects in the crystals; reflectance spectrum from guanine crystal multilayers with the same cytoplasm spacing and different layer number; the normalized standard silvery reflection spectrum in nature; and electric field strength distribution in the sampled actual multilayer structure without crystal defects (PDF)

AUTHOR INFORMATION

Corresponding Authors

Zhengdong Cheng – *Wenzhou Institute, Wenzhou Key Laboratory of Biophysics, University of Chinese Academy of Sciences, Wenzhou, Zhejiang 325001, China*; Email: zcheng01@zju.edu.cn

Jianwei Shuai – *Wenzhou Institute, Wenzhou Key Laboratory of Biophysics, University of Chinese Academy of Sciences, Wenzhou, Zhejiang 325001, China*; orcid.org/0000-0002-8712-0544; Email: jianweishuai@xmu.edu.cn

Authors

Jinjin Zhong – *Wenzhou Institute, Wenzhou Key Laboratory of Biophysics, University of Chinese Academy of Sciences,*

https://doi.org/10.1021/acsanm.4c00252
ACS Appl. Nano Mater. 2024, 7, 6487–6498

Wenzhou, Zhejiang 325001, China; orcid.org/0000-0002-9782-9354

Ling Li − *Department of Mechanical Engineering, Virginia Tech, Blacksburg, Virginia 24060, United States;* orcid.org/0000-0002-6741-9741

Sarah Kariko − *Museum of Comparative Zoology, Harvard University, Cambridge, Massachusetts 02318, United States*

Long Zhang − *Department of Physics, Xiamen University, Xiamen, Fujian 361005, China*

Zhengyong Song − *Department of Electronic Science, Xiamen University, Xiamen, Fujian 361005, China;* orcid.org/0000-0002-3575-3243

Xiang Li − *Department of Physics, Xiamen University, Xiamen, Fujian 361005, China*

Yuer Lu − *Wenzhou Institute, Wenzhou Key Laboratory of Biophysics, University of Chinese Academy of Sciences, Wenzhou, Zhejiang 325001, China*

Complete contact information is available at: https://pubs.acs.org/10.1021/acsanm.4c00252

Funding

This work is supported by the STI2030-Major Projects 2021ZD0201900 to J.S., the National Natural Science Foundation of China (Grant No. 12090052 to J.S.), and the Wenzhou Institute, University of Chinese Academy of Sciences' startup fund WIUCASQD2023007 to J.Z.

Notes

The authors declare no competing financial interest.

■ ACKNOWLEDGMENTS

The authors extend their sincere gratitude to Dr. Richard Schalek of Prof. Jeff W. Lichtman's research team at Harvard University for his invaluable support with the serial sectioning and electron microscopy imaging procedures. S.K. is thankful for the assistance provided by the Invertebrate Zoology Collections at the Museum of Comparative Zoology, including Curators Charles Griswold and Lauren Esposito, and also expresses appreciation to Darrell Ubick and Anthea Carmichael of the California Academy of Sciences for the specimen loans.

■ REFERENCES

(1) Gur, D.; Palmer, B. A.; Weiner, S.; Addadi, L. Light Manipulation by Guanine Crystals in Organisms: Biogenic Scatterers, Mirrors, Multilayer Reflectors and photonic Crystals. *Adv. Funct. Mater.* **2017**, *27*, No. 1603514.

(2) Iwasaka, M.; Mizukawa, Y. Light Reflection Control in Biogenic Micro-Mirror by Diamagnetic Orientation. *Langmuir* **2013**, *29*, 4328−4334.

(3) Zeng, M.; King, D.; Huang, D.; Do, C.; Wang, L.; Chen, M.; Lei, S.; Lin, P.; Chen, Y.; Cheng, Z. Iridescence in Nematics: photonic Liquid Crystals of nanoplates in Absence of Long-Range Periodicity. *P. Natl. Acad. Sci. USA* **2019**, *116*, 18322−18327.

(4) Iwasaka, M.; Mizukawa, Y.; Roberts, N. W. Magnetic Control of the Light Reflection Anisotropy in a Biogenic Guanine Microcrystal Platelet. *Langmuir* **2016**, *32*, 180−187.

(5) Fudouzi, H. Tunable Structural Color in Organisms and photonic Materials for Design of Bioinspired Materials. *Sci. Technol. Adv. Mater.* **2011**, *12*, No. 064704.

(6) Iwasaka, M. Effects of Static Magnetic Fields on Light Scattering in Red Chromatophore of Goldfish Scale. *J. Appl. Phys.* **2010**, *107*, No. 09B314.

(7) Iwasaka, M., Magnetic Control of Biogenic Micro-Mirror. In *Bioimaging*; CRC Press: 2020; pp 215−232.

(8) Iwasaka, M.; Asada, H. Floating photonic Crystals Utilizing Magnetically Aligned Biogenic Guanine Platelets. *Sci. Rep-UK* **2018**, *8*, 16940.

(9) Mizukawa, Y.; Iwasaka, M. Magnetic Orientational Tweezers for Cell Manipulation. *Trans. Jpn. Soc. Med. Biol. Eng.* **2013**, *51*, M-127.

(10) Mootha, A.; Suzuki, K.; Kimura, T.; Kurahashi, M.; Muneyama, E.; Iwasaka, M.; Asada, H. Refinement of Synthetic Guanine Crystals for Fast Diamagnetic Rotation. *AIP Adv.* **2019**, *9*, No. 035340.

(11) Sogame, T.; Deguchi, K.; Kimura, T.; Muneyama, E.; Inoue, M.; Asada, H.; Iwasaka, M.; Kishimoto, K.; Koyanagi, T. Fabrication of Biogenic Guanine Crystal/Ferromagnetic Film Hybrid Plate for Micro-Optical Micro-Electromechanical Systems. *IEEE Trans. Magn.* **2018**, *54*, 1−4.

(12) Levy-Lior, A.; Shimoni, E.; Schwartz, O.; Gavish-Regev, E.; Oron, D.; Oxford, G.; Weiner, S.; Addadi, L. Guanine-Based Biogenic photonic-Crystal Arrays in Fish and Spiders. *Adv. Funct. Mater.* **2010**, *20*, 320−329.

(13) Palmer, B. A.; Taylor, G. J.; Brumfeld, V.; Gur, D.; Shemesh, M.; Elad, N.; Osherov, A.; Oron, D.; Weiner, S.; Addadi, L. The Image-Forming Mirror in the Eye of the Scallop. *Science* **2017**, *358*, 1172−1175.

(14) Dearden, S. J.; Ghoshal, A.; DeMartini, D. G.; Morse, D. E. Sparkling Reflective Stacks of Purine Crystals in the Nudibranch Flabellina iodinea. *Biological Bulletin* **2018**, *234*, 116−129.

(15) Zhang, G.; Yallapragada, V. J.; Shemesh, M.; Wagner, A.; Upcher, A.; Pinkas, I.; McClelland, H. L.; Hawlena, D.; Palmer, B. A. Ontogenetic Color Switching in Lizards as a by-Product of Guanine Cell Development. *bioRxiv* **2022**, 2022-01.

(16) Gur, D.; Leshem, B.; Oron, D.; Weiner, S.; Addadi, L. The Structural Basis for Enhanced Silver Reflectance in Koi Fish Scale and Skin. *J. Am. Chem. Soc.* **2014**, *136*, 17236−17242.

(17) Feller, K. D.; Jordan, T. M.; Wilby, D.; Roberts, N. W. Selection of the Intrinsic Polarization Properties of Animal Optical Materials Creates Enhanced Structural Reflectivity and Camouflage. *Philos. T. R. Soc. B* **2017**, *372*, No. 20160336.

(18) Jordan, T. M.; Partridge, J. C.; Roberts, N. W. Non-Polarizing Broadband Multilayer Reflectors in Fish. *Nat. Photonics* **2012**, *6*, 759−763.

(19) Zhong, J.; Song, Z.; Zhang, L.; Li, X.; He, Q.; Lu, Y.; Kariko, S.; Shaw, P.; Liu, L.; Ye, F.; Li, L.; Shuai, J. Assembly of Guanine Crystals as a Low-Polarizing Broadband Multilayer Reflector in a Spider, Phoroncidia Rubroargentea. *ACS Appl. Mater. Interfaces* **2022**, *14*, 32982−32993.

(20) Gur, D.; Leshem, B.; Farstey, V.; Oron, D.; Addadi, L.; Weiner, S. Light-Induced Color Change in the Sapphirinid copepods: Tunable photonic Crystals. *Adv. Funct. Mater.* **2016**, *26*, 1393−1399.

(21) Gur, D.; Leshem, B.; Pierantoni, M.; Farstey, V.; Oron, D.; Weiner, S.; Addadi, L. Structural Basis for the Brilliant Colors of the Sapphirinid copepods. *J. Am. Chem. Soc.* **2015**, *137*, 8408−8411.

(22) Teyssier, J.; Saenko, S. V.; Van Der Marel, D.; Milinkovitch, M. C. photonic Crystals Cause Active Colour Change in Chameleons. *Nat. Commun.* **2015**, *6*, 6368.

(23) Gur, D.; Palmer, B. A.; Leshem, B.; Oron, D.; Fratzl, P.; Weiner, S.; Addadi, L. The Mechanism of Color Change in the Neon Tetra Fish: A Light-Induced Tunable photonic Crystal Array. *Angew. Chem., Int. Ed.* **2015**, *54*, 12426−12430.

(24) Hirsch, A.; Gur, D.; Polishchuk, I.; Levy, D.; Pokroy, B.; Cruz-Cabeza, A. J.; Addadi, L.; Kronik, L.; Leiserowitz, L. Guanigma": The Revised Structure of Biogenic Anhydrous Guanine. *Chem. Mater.* **2015**, *27*, 8289−8297.

(25) Levy-Lior, A.; Pokroy, B.; Levavi-Sivan, B.; Leiserowitz, L.; Weiner, S.; Addadi, L. Biogenic Guanine Crystals from the Skin of Fish May Be Designed to Enhance Light Reflectance. *Cryst. Growth Des.* **2008**, *8*, 507−511.

(26) Lythgoe, J.; Shand, J. Changes in Spectral Reflexions from the Iridophores of the Neon Tetra. *Journal of physiology* **1982**, *325*, 23−34.

(27) Yoshioka, S.; Matsuhana, B.; Tanaka, S.; Inouye, Y.; Oshima, N.; Kinoshita, S. Mechanism of Variable Structural Colour in the

Neon Tetra: Quantitative Evaluation of the Venetian Blind Model. *J. Royal Soc. Interface* **2011**, *8*, 56−66.
(28) CLOTHIER, J.; Lythgoe, J. Light-Induced Colour Changes by the Iridophores of the Neon Tetra, Paracheirodon Innesi. *J. Cell Sci.* **1987**, *88*, 663−668.
(29) Kariko, S.; Timonen, J. V.; Weaver, J. C.; Gur, D.; Marks, C.; Leiserowitz, L.; Kolle, M.; Li, L. Structural Origins of Coloration in the Spider Phoroncidia Rubroargentea Berland, 1913 (Araneae: Theridiidae) from Madagascar. *J. Royal Soc. Interface* **2018**, *15*, No. 20170930.
(30) Kimura, T.; Takasaki, M.; Hatai, R.; Nagai, Y.; Uematsu, K.; Oaki, Y.; Osada, M.; Tsuda, H.; Ishigure, T.; Toyofuku, T.; Shimode, S.; Imai, H. Guanine Crystals Regulated by Chitin-Based Honeycomb Frameworks for Tunable Structural Colors of Sapphirinid Copepod, Sapphirina Nigromaculata. *Sci. Rep.* **2020**, *10*, 2266.
(31) Gur, D.; Nicolas, J. D.; Brumfeld, V.; Bar-Elli, O.; Oron, D.; Levkowitz, G. The Dual Functional Reflecting Iris of the Zebrafish. *Adv. Sci.* **2018**, *5*, No. 1800338.
(32) Land, M. A Multilayer Interference Reflector in the Eye of the Scallop, Pecten Maximus. *J. Exp. Biol.* **1966**, *45*, 433−447.
(33) Warrant, E. J. Visual Optics: Remarkable Image-Forming Mirrors in Scallop Eyes. *Curr. Biol.* **2018**, *28*, R262−R264.
(34) Mueller, K. P.; Labhart, T. Polarizing Optics in a Spider Eye. *J. Comp. Physiol. A* **2010**, *196*, 335−348.
(35) Fenk, L. M.; Schmid, A. The Orientation-Dependent Visual Spatial Cut-Off Frequency in a Spider. *J. Exp. Biol.* **2010**, *213*, 3111−3117.
(36) Morehouse, N. Spider Vision. *Curr. Biol.* **2020**, *30*, R975−R980.
(37) Politi, Y.; Bertinetti, L.; Fratzl, P.; Barth, F. G. The Spider Cuticle: A Remarkable Material Toolbox for Functional Diversity. *Philos. T. R. Soc. A* **2021**, *379*, No. 20200332.
(38) Land, M. F. Eyes with Mirror Optics. *J. Opt. A-Pure Appl. Op.* **2000**, *2*, R44.
(39) Lythgoe, J.; SHAND, J. The Structural Basis for Iridescent Colour Changes in Dermal and Corneal Irddophores in Fish. *J. Exp. Biol.* **1989**, *141*, 313−325.
(40) Wagner, A.; Ezersky, V.; Maria, R.; Upcher, A.; Lemcoff, T.; Aflalo, E. D.; Lubin, Y.; Palmer, B. A. The Non-Classical Crystallization Mechanism of a Composite Biogenic Guanine Crystal. *Adv. Mater.* **2022**, *34*, No. e2202242.
(41) Hirsch, A.; Palmer, B. A.; Elad, N.; Gur, D.; Weiner, S.; Addadi, L.; Kronik, L.; Leiserowitz, L. Biologically Controlled Morphology and Twinning in Guanine Crystals. *Angew. Chem., Int. Ed.* **2017**, *56*, 9420−9424.
(42) Guo, D.; Liu, Y.; Hou, X.; Wang, X.; Fan, C.; Bao, L.; He, X.; Zhang, H.; Ma, Y. Formation Mechanism of Twinned β-Form Anhydrous Guanine Platelets in Scallop Eyes. *CrystEngComm* **2023**, *25*, 4521−4530.
(43) Wagner, A.; Upcher, A.; Maria, R.; Magnesen, T.; Zelinger, E.; Raposo, G.; Palmer, B. A. Macromolecular Sheets Direct the Morphology and Orientation of Plate-Like Biogenic Guanine Crystals. *Nat. Commun.* **2023**, *14*, 589.
(44) Jantschke, A.; Pinkas, I.; Hirsch, A.; Elad, N.; Schertel, A.; Addadi, L.; Weiner, S. Anhydrous B-Guanine Crystals in a Marine Dinoflagellate: Structure and Suggested Function. *J. Struct. Biol.* **2019**, *207*, 12−20.
(45) Aizen, R.; Tao, K.; Rencus-Lazar, S.; Gazit, E. Functional Metabolite Assemblies—a Review. *J. Nanopart. Res.* **2018**, *20*, 1−9.
(46) Wagner, A.; Ezersky, V.; Maria, R.; Upcher, A.; Lemcoff, T.; Aflalo, E. D.; Lubin, Y.; Palmer, B. A. The Non-Classical Crystallization Mechanism of a Composite Biogenic Guanine Crystal. *Adv. Mater.* **2022**, *34*, No. 2202242.
(47) Pinsk, N.; Wagner, A.; Cohen, L.; Smalley, C. J. H.; Hughes, C. E.; Zhang, G.; Pavan, M. J.; Casati, N.; Jantschke, A.; Goobes, G.; Harris, K. D. M.; Palmer, B. A. Biogenic Guanine Crystals Are Solid Solutions of Guanine and Other Purine Metabolites. *J. Am. Chem. Soc.* **2022**, *144*, 5180−5189.
(48) Land, M. F. The Physics and Biology of Animal Reflectors. *Prog. Biophys. Mol. Biol.* **1972**, *24*, 75−106.
(49) Chinta, S. P.; Goller, S.; Uhl, G.; Schulz, S. Identification and Synthesis of Branched Wax-Type Esters, Novel Surface Lipids from the Spider Argyrodes Elevatus (Araneae: Theridiidae). *Chem. Biodiversity* **2016**, *13*, 1202−1220.
(50) McKenzie, D. R.; Yin, Y.; McFall, W. D. Silvery Fish Skin as an Example of a Chaotic Reflector. *Proc. R. Soc. London, Ser. A* **1995**, *451*, 579−584.
(51) Jordan, T. M.; Partridge, J.; Roberts, N. Disordered Animal Multilayer Reflectors and the Localization of Light. *J. Royal Soc. Interface* **2014**, *11*, No. 20140948.
(52) Zhao, S.; Brady, P. C.; Gao, M.; Etheredge, R. I.; Kattawar, G. W.; Cummings, M. E. Broadband and Polarization Reflectors in the Lookdown, Selene Vomer. *J. Royal Soc. Interface* **2015**, *12*, No. 20141390.
(53) Feng, M.; Feng, Y.; Zhang, T.; Li, J.; Chen, Q.; Chi, Q.; Lei, Q. Recent Advances in Multilayer-Structure Dielectrics for Energy Storage Application. *Adv. Sci.* **2021**, *8*, No. 2102221.
(54) Cho, H. J.; Kim, S. J.; Kim, K. D.; Cho, S. P.; Tak, I. S.; Kim, G. H.; Moon, B. J.; Kim, D. H.; Lee, Y. S.; Kim, S. I.; Kim, H. T.; Cho, J. Simply Structured Polarization-Independent High Efficiency Multilayer Dielectric Gratings. *Appl. Opt.* **2022**, *61*, 8446−8453.
(55) Dacke, M.; Nilsson, D.-E.; Warrant, E.; Blest, A.; Land, M.; O'carroll, D. Built-in Polarizers Form Part of a Compass Organ in Spiders. *Nature* **1999**, *401*, 470−473.

https://doi.org/10.1021/acsanm.4c00252
ACS Appl. Nano Mater. 2024, 7, 6487−6498